Eur. Phys. J. B **38**, 3–8 (2004)
DOI: 10.1140/epjb/e2004-00091-3

THE EUROPEAN PHYSICAL JOURNAL B

Experimental test of a superconducting digital interface for vortex qubits

V.K. Kaplunenko[1] and A.V. Ustinov[2,a]

[1] Superconductor Technologies Inc., 969 West Maude Avenue, Sunnyvale, CA 94086, USA
[2] Physikalisches Institut III, Universität Erlangen-Nürnberg, Erwin-Rommel-Str. 1, 91058 Erlangen, Germany

Received 16 January 2004
Published online 20 April 2004 –

Abstract. We have developed and tested a classical superconducting logic interface to a qubit prototype based on two macroscopically distinct quantum states of a vortex in a long Josephson junction. The initial state preparation as well as the readout of a qubit is demonstrated by using a relatively simple Rapid Single Flux Quantum (RSFQ) circuit. RSFQ logic appears as a very feasible choice for constructing an interface between superconducting qubits and room-temperature electronics.

PACS. 74.40.+k Fluctuations (noise, chaos, nonequilibrium superconductivity, localization, etc.) – 74.50.+r Tunneling phenomena; point contacts, weak links, Josephson effects – 74.78.-w Superconducting films and low-dimensional structures

1 Introduction

Most qubits have been implemented thus far in various microscopic physical systems such as atoms in cavities, ions in traps, photons, and ensembles of nuclear spins. These microscopic systems have an advantage of relatively easy isolation from the environment, which is needed to reduce decoherence. The common disadvantage of microscopic systems is that their physical properties are given by nature and cannot be tailored. This limits the design flexibility of a prospective quantum computer. Thus the integration of many microscopic qubits into a more complex circuit like a practical computer becomes a formidable task.

Macroscopic (or at least mesoscopic) quantum systems offer much more flexibility to design a quantum computer based on standard integrated circuit fabrication technologies. A variety of solid state quantum systems has been recently proposed for use as qubits. Most of them are based on nano-structured electronic circuits using either quantum dots or tunnel junctions as two-level systems. These circuits can be implemented in a chip-based technology using modern lithography techniques that in turn offer design flexibility and the ability to scale up the number of qubits. Such solid state systems are more similar in fabrication and in operation to conventional computers than any of the microscopic qubits. However, it is difficult to isolate such a macroscopic quantum system from the environment, and therefore, they are more prone to decoherence.

The most promising macroscopic qubits, which have been demonstrated *experimentally*, are based on superconducting Josephson tunnel junctions [1]. Superconducting qubits take an advantage of the intrinsic coherence of the superconducting condensate, from which dissipative electronic excitations are separated by an energy gap. The gap must be larger than the typical operating temperature of the qubit. There are two main types of superconducting qubits: charge qubits, and flux qubits. Recently several new implementations of such qubits have been proposed and tested. These are charge-flux qubit [2] (called also quantronium), and phase qubits [3,4].

The charge states of a superconducting island coupled to a reservoir through a small tunnel junction are used as the basis states of the charge qubit. The first experiment performed by Nakamura et al. demonstrated the superposition of charge states and the coherent oscillations between two of them [5]. The following experiments have clearly shown Rabi flopping [6], and charge echo [7] with a decoherence time of the order of few nanoseconds.

The flux qubits are based on the quantum dynamics governed by magnetic flux and persistent currents in loops with Josephson junctions. Flux qubits have larger size than charge qubits, which makes them easier to fabricate and test. These qubits do not necessarily require microwaves for preparing a two-level state, which is definitely a practical advantage of flux qubits over the recently demonstrated pure phase qubits based on single Josephson junctions. The quantum superposition of different magnetic flux states in SQUID-based flux qubits has been reported in [8,9], and very recently the quantum-coherent flux oscillations in flux qubits have been observed [10].

However we are interested in a special type of flux qubit called the vortex qubit. The vortex qubit has been proposed earlier [11–13] and is based on two spatially

[a] e-mail: ustinov@physik.uni-erlangen.de

distinct macroscopic quantum states of a vortex in a long Josephson junction (LJJ). In order to form the qubit, the vortex is trapped in a specially prepared double-well potential inside an LJJ. The potential in an LJJ can be formed by using a non-uniform magnetic field. A desired field profile can be achieved, e.g., by tailoring the junction shape [11]. The amplitude of the potential can be varied by tuning the external magnetic field. At sufficiently low temperatures, vortices are predicted to behave as macroscopic quantum particles [14,15]. The quantum effects occur due to the smallness of the vortex effective mass, which is proportional to the width W of the junction. For a width of $W = 1\,\mu$m the vortex effective mass is about $10^{-3}m_e$, where m_e is the electron mass. Quantum tunneling of vortices has been previously observed in discrete arrays of small Josephson junctions [16]. Recently, the Erlangen group has for the first time experimentally demonstrated the quantum tunneling of a single vortex in LJJ and measured its energy levels in the trapping potential well [17].

In this paper, we report the results of testing a prototype of the vortex qubit in combination with a classical logic interface, which is used for initializing and reading out the qubit states. As the classical shell we have chosen superconducting digital Rapid Single Flux Quantum (RSFQ) logic [18]. The main motivations of using RSFQ logic was the fabrication process compatibility, and its similarity to superconducting qubit operation regimes. The superconducting RSFQ logic family is considered as one of the emerging digital technologies for next generation electronics.

The paper is organized as follows. First, we describe a modified vortex qubit based on local field injectors. Then we discuss the principle of RSFQ circuit interface, which we propose for qubit state preparation, and for reading out the result of quantum computation. Finally, we present the layout of the fabricated circuit and report results of its experimental testing at 4.2 K. The paper is concluded by discussing the feasibility and possible limitations of the operation of the proposed RSFQ interface with vortex qubits at millikelvin temperatures.

2 Vortex qubit in a long Josephson junction with local field injectors

We propose a modified design of a vortex qubit, which is suitable for combination with classical superconducting RSFQ logic. The proposed qubit is illustrated by Figure 1. We suggest to use *local field injectors* as an alternative to the shape tailoring of LJJ as was proposed previously [11–13].

The schematic view of the modified vortex qubit is shown in Figure 1a. A double-well potential for the vortex is formed by local magnetic fields produced by two control lines carrying the currents I_1 and I_2. The current I_1 is used to induce a local magnetic field that produces a wide potential minimum for the vortex, while the current I_2 generates a local energy barrier dividing the trap in two potential wells (A and B in Fig. 1.) Figure 1b illustrates

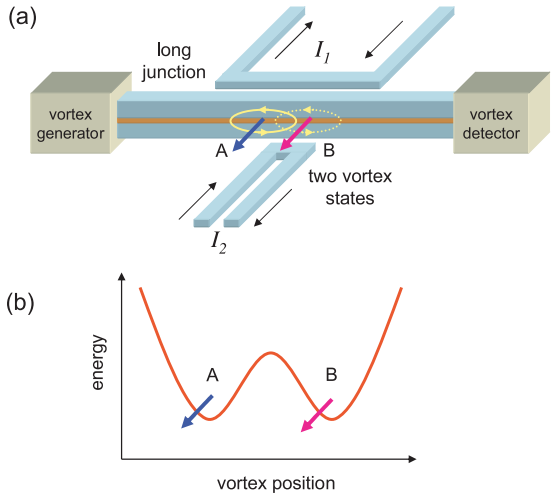

Fig. 1. (a) Schematic view of a vortex qubit based on local magnetic field injectors. (b) Double-well potential for a vortex formed by injectors in the structure above. A and B mark two vortex states.

the vortex potential shape generated by these currents. The qubit can be manipulated by varying the currents I_1 and I_2 as well as the uniform bias current I_B, which can be used to tilt the potential.

To quantitatively estimate the possible potential shape, we analytically calculated the vortex interaction potential as a function of injector currents. The perturbed sine-Gordon equation [19] written in normalized units was used to calculate the vortex potential, which was induced by a δ-function like current injector:

$$U(x, y, \varepsilon) = -\varepsilon \arctan e^{x-y}, \tag{1}$$

where x is the coordinate of the fluxon center of mass, y is the position of the fluxon injector, and $\varepsilon = I_{\rm inj}/(J_c\lambda_J)$ is the normalized injector current. The effective potential of the LJJ with four current injectors can be written as:

$$W = U\left(-\frac{d_1}{2}, \varepsilon_1\right) + U\left(\frac{d_1}{2}, -\varepsilon_1\right) + U\left(-\frac{d_2}{2}, \varepsilon_2\right) + U\left(\frac{d_2}{2}, -\varepsilon_2\right), \tag{2}$$

where d_1 and d_2 are the spacings between the pairs of current injectors, and ε_1 and ε_2 are the injectors normalized currents.

Figure 2 shows the vortex energy profile obtained for a particular distance between current injectors $d_1 = 3$, and $d_2 = 1$, which are carrying normalized currents $\varepsilon_1 = 0.8$, and $\varepsilon_2 = -1.3$ given by equation (2). Calculations show that the current variation ε_2 in the range from -3 to 0 continuously reduces the barrier to zero and modifies the potential profile from the double-well to the single-well form.

The tunnel splitting of this qubit should be similar to that of heart-shaped LJJ vortex qubit calculated in WKB approximation reference [13]. The tunneling rate can be

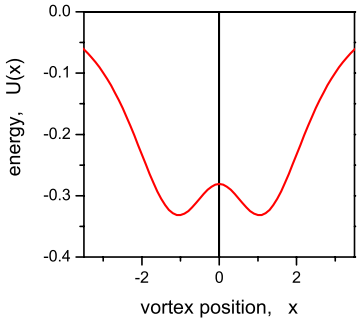

Fig. 2. Double-well potential of the vortex calculated from equation (2).

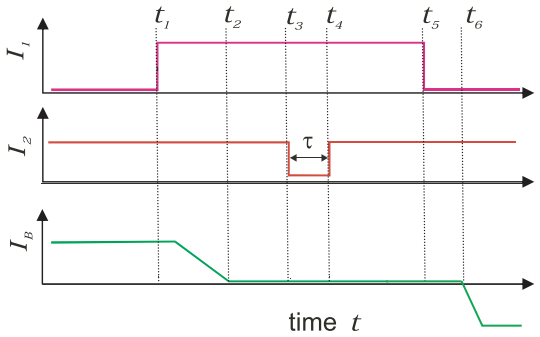

Fig. 3. Time diagram of the measurement cycle in the proposed experiment.

tuned within the experimentally accessible range by about four orders of magnitude between 10^{-5} and 10^{-9} s. The decoherence of the proposed qubit is expected to be similar to that of other flux qubits and phase qubits based on Josephson junctions, which should be extendable under optimal experimental conditions up to μs time range.

3 RSFQ circuit for vortex qubit initialization and readout

The goal of the experiment with the qubit in Figure 1 is the observation of the coherent oscillations of the vortex between two wells. The lowest energy eigenstates for a vortex in a double-well potential were calculated earlier [13], and showed that the typical frequency of such oscillations $f_{\rm coher}$ can be tuned in the range between 100 kHz and 1 GHz. The frequency $f_{\rm coher}$ depends on the height of the potential barrier $\sim I_2$ between wells A and B (see Fig. 1).

To measure the coherent oscillations we propose to use vortex manipulation with a technique similar to that used by Nakamura et al. [5] in an experiment with Cooper pairs. Specifically, we would like to measure the probability of vortices to be in one of the states (for example, well B) as a function of the time interval τ during which the superposition of two states takes place. The superposition is set by reducing the height of the barrier between the wells. The measurement procedure includes initial state preparation of the vortex qubit, formation of a quantum superposition of two classically separated states over the chosen time interval τ, and reading out of the final qubit state. The quantum superposition state of the qubit is terminated by increasing the height of the barrier between the wells. This results in a qubit state in which the vortex is positioned either in well A (state $|0\rangle$) or in well B (state $|1\rangle$), depending on both frequency $f_{\rm coher}$ and time τ. By repeating this procedure many times for different τ, it should be possible to observe oscillations of the probability of finding the vortex in one of the wells with the time period of $1/f_{\rm coher}$.

To prepare the initial state of the qubit, a single flux quantum (SFQ) generator is attached to one side of LJJ, as it is shown schematically in Figure 1. The generator can be either the standard RSFQ dc-to-SFQ cell, or a vortex injector [20] furnished with an antivortex absorber. The SFQ (vortex) generator circuit turns the input current rise into a vortex that is sent to the underdamped LJJ. When the vortex enters LJJ, a locally applied magnetic field generated by current I_2 forms a repulsive potential that traps the arriving vortex in the region $|0\rangle$. Then the local current I_1 is switched on($I_1 > I_2$) and, due to the opposite orientations of the magnetic fields generated by currents I_1 and I_2, a double-well potential for the vortex is formed. Initially, the current I_2 is kept high so that the vortex is classically sitting in the well A (state $|0\rangle$).

After the qubit is initialized, the current I_2 is reduced to a smaller level and remains unchanged for a short time τ. The appropriate current level is chosen such that the lowest energy eigenstate of the vortex splits into two levels separated by the energy difference, which is proportional to the chosen frequency of coherent oscillations $f_{\rm coher}$. After the time τ is over, the current I_2 is raised again and the vortex has a certain probability to be found in either well A or well B. If the quantum decoherence time $t_{\rm dec}$ is larger than τ, the probability of finding the vortex in one of the wells should oscillate as a function of τ, with the period of $1/f_{\rm coher}$. Thus we can measure quantum coherent oscillations between two degenerate states using a time domain approach. The final state of the vortex is read out by reducing the current I_1 to zero level. This sends the vortex either to the left or the right side of the LJJ, depending on its state. The vortex motion can be additionally facilitated by switching on a small uniform bias current in the long junction, which moves the vortex to an SFQ counter attached to another side of LJJ, see Figure 1a. The vortex will move there and hence be counted only if located at the well B (state $|1\rangle$). If the vortex is located in the well A (state $|0\rangle$), it will remain there due to the large potential barrier formed by current I_2. The LJJ is reset to its original state (vortex-free) by applying a negative bias current that removes the vortex from well A through the RSFQ buffer stage, which should be a part of the RSFQ source shown in Figure 1a.

Figure 3 presents the time diagram of the measurement cycle. At the time t_1 the vortex gets locked in the potential well A. The potential tilt is removed at $t = t_2$ by turning the bias current $I_{\rm B}$ to zero. The quantum superposition is switched on at $t = t_3$ and off at $t = t_4$. The current I_1

switches off at $t = t_5$. Thus if the vortex is located at well B it will move to the right and reach the counter. A small negative bias current I_B is turned on at $t = t_6$. It removes the vortex, when trapped in well A, through the input buffer stage. After that the system is reset to its initial state.

4 Circuit layout and simulation

To test the measurement procedure described in the previous section, we have developed a circuit combining a vortex qubit prototype with an RSFQ interface.

Figure 4 shows the layout of the circuit. The vortex qubit prototype is located in the central part of the circuit. The anti-vortex absorber is a resistor, which prevents vortex reflection at the end of the LJJ. The vortex injector is implemented by using a superconducting transformer, which is galvanically isolated from the LJJ. The current applied across the transformer sends a vortex to the right and leaves behind an anti-vortex in the injector. The system returns to its initial state when the current across the transformer is decreased, because as result of that the anti-vortex moves to the absorber and disappears. After the superposition of two states the vortex can be found in one of two states, A or B. If it is on the right side of the barrier (well B) it will raise the voltage on the readout RS-flip-flop during the readout process, and that voltage can be detected by any kind of voltmeter. Vortex appearance on the left (well A) is not detected as the circuit is reset by sending the vortex back to the absorber.

The whole circuit was simulated and optimized using the Superconducting Schematic Editor and Simulator WINS [21]. The circuit was found successfully functioning with layout margins of about 29% and bias current margins of 15%.

The circuit was fabricated using standard Nb trilayer technology [22]. The RSFQ Josephson junctions have the critical current density $j_c = 1000\,\mathrm{A/cm^2}$, the junction area of $5 \times 5\,\mu\mathrm{m}^2$ with $I_c = 250\,\mu\mathrm{A}$, shunt resistance $R_\mathrm{N} = 1.2\,\Omega$ and characteristic voltage of $V_C \approx I_C R_\mathrm{N} = 300\,\mu\mathrm{V}$. This fabrication technology has achieved the complexity of up to ~6000 junctions per chip, and has demonstrated maximum clock rates up to 20 GHz.

The picture of the fabricated and tested circuit is shown in Figure 5. Figure 6 shows the enlarged image of the area of the qubit prototype where the double-well potential is formed. Note that an extra loop (in a picture it looks as a hole) was used as a transformer to create a potential for the vortex. In order to reduce possible electromagnetic interference, this transformer is also galvanically isolated from the LJJ.

5 Test of RSFQ qubit interface operation

In order to observe coherent oscillations, the vortex qubit has to be measured in the quantum regime at temperatures below 100 mK. So far we report testing of the developed circuit in the classical regime at 4.2 K, when only

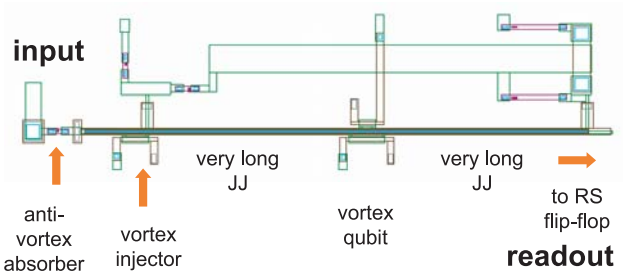

Fig. 4. A fragment the vortex qubit layout developed and tested in combination with the RSFQ readout circuit.

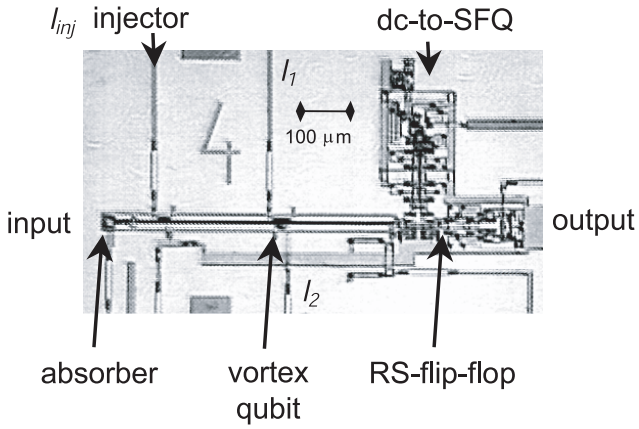

Fig. 5. Photo of the tested circuit. Extra dc-to-SFQ converter was used to set RS-flip-flop. This test sample was fabricated using Hypres, Inc. foundry

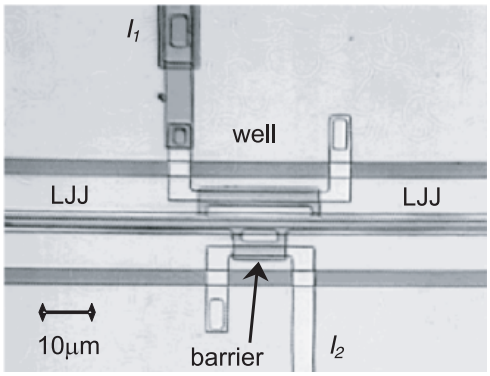

Fig. 6. Photograph of the prototype of vortex qubit located in the central part of Figure 5. This part of the circuit creates a double-well potential for the vortex.

thermal fluctuations can move vortex between wells in the double-well potential. Thus the probabilities to find vortex in each of two wells should be equal.

Figure 7 demonstrates the functionality of the interface between the LJJ and RSFQ circuit, and free vortex propagation along the LJJ. First, the I_set current switches an RS-flip-flop to the voltage state. Then the I_inj kicks the vortex into the LJJ. The vortex pass the whole LJJ and its arrival to the output counter switches the flip-flop back to the zero voltage state. The margin of injector current I_inj was rather narrow, so for future development we propose

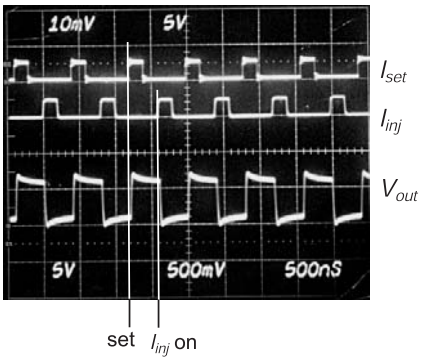

Fig. 7. RSFQ oscillograms of the test circuit measured at 4.2 K. Vortex freely moves from injector to RS-flip-flop along LJJ with no potential barrier. The repetition rate is set by $I_{\rm set}$ pulses. The switching of $I_{\rm inj}$ sends vortex to LJJ. The output amplitude of RS-flip-flop is 0.3 mV. Common bias current $I_{\rm bias}$ is 5.4 mA (margin from 4.88 to 5.92 mA). Injector current $I_{\rm inj}$ has margins of about 3%, the injector adjustment current $I_{\rm Ladj}$ can vary from –0.115 mA to 0.55 mA, and LJJ right edge adjustment current $I_{\rm Radj}$ from –0.58 mA to 0.77 mA.

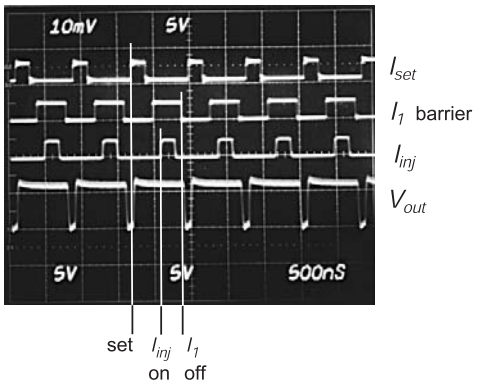

Fig. 8. RSFQ oscillograms of the test circuit measured at 4.2 K. Vortex captured by the potential barrier induced by the current I_1. The bias current is $I_{\rm bias}$ = 5.4 mA (margin from 4.81 to 5.77 mA); injector current has margins of 3%, $I_{\rm Ladj}$ = −0.265 mA with margin from –0.045 to –0.495 mA; $I_{\rm Radj}$ = 0 mA. The barrier amplitude is I_1 = 8.6 mA and has margins from 4.4 to 9.8 mA.

to use a dc-to-SFQ converter instead of a transformer. In contrast, the interface to flip-flop has large enough margins that prove its feasibility.

The next step was to trap the vortex in the double well region using the control currents I_1 and I_2. Figure 8 shows the result of such an experiment using I_1. First, the RS-flip-flop is set to the voltage state. Then a positive current I_1 is applied to create the potential barrier for the vortex. After that the injector sends the vortex to the LJJ. The following event is clearly different from the one shown in Figure 7. Now the flip-flop switches to the zero voltage step only when barrier released the vortex ("I_1 off"). As expected, similar behavior was found for the current I_2 injected in the opposite direction, as in Figure 9.

By setting I_1 to a negative value we have also been able to trap the vortex in the potential well. This kind of measurement is presented in Figure 10. The additional

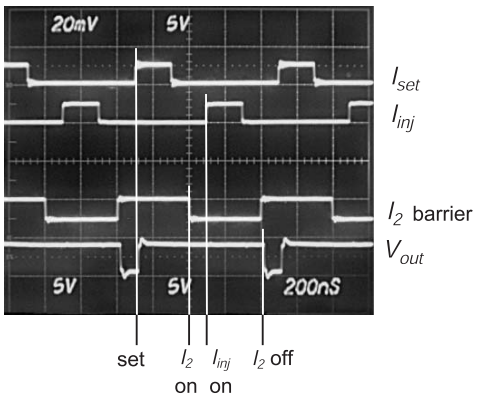

Fig. 9. RSFQ oscillograms of the test circuit measured at 4.2 K. Vortex is trapped by a barrier formed by current I_2. $I_{\rm bias}$ = 5.5 mA (margins from 4.81 to 5.77 mA); $I_{\rm Ladj}$ = −0.675 mA and $I_{\rm Radj}$ = 0 mA. The barrier of I_2 has margins from –10.15 to more than –2 mA.

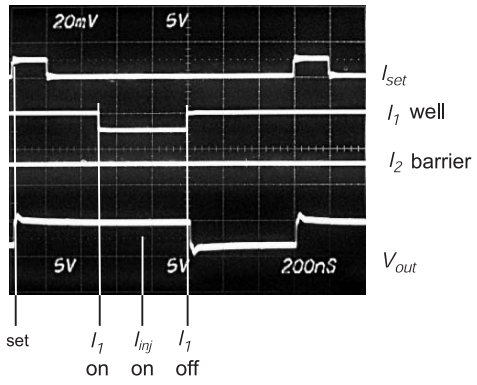

Fig. 10. RSFQ oscillograms of the test circuit measured at 4.2 K. Vortex is trapped in the well created by negative current I_1. The bias is $I_{\rm bias}$ = 5.51 mA; $I_{\rm Ladj}$ = −0.075 mA; $I_{\rm Radj}$ = 0.615 mA. The amplitude of I_1 is –2.05 mA. The injector current trace is not shown.

tests have shown that it is also possible to trap a vortex in the double well potential, and even observe thermally activated jumps of the vortex between wells. The operating margins were found to be low, as can be expected. Data analysis have shown that due to the finite width of the injection leads each well is reduced in width to about 8 μm. The Josephson penetration depth λ_J in this sample is about 12 μm. In order to manipulate the vortex between two wells it is necessary to slightly broaden the main well by increasing the distance between I_1 transformer leads.

6 Discussion

Superconducting RSFQ logic is a very suitable digital technology for an interface between superconducting qubits and room-temperature electronics. It has very low power consumption: about four orders of magnitude less than advanced semiconductor circuits. RSFQ is extremely fast and the 20 GHz level achieved with the current fabrication technologies is not a physical limitation. The external communication between RSFQ and

room-temperature semiconductor electronics can be realized by using optical fiber channels combined with metal-semiconductor-metal stages at the input and laser-emitting diodes at the output.

The true vortex qubit experiment has to be performed at millikelvin temperatures. To match this requirement, the RSFQ circuit should be optimized for low power consumption. The main power dissipation in RSFQ circuit is due to the bias resistors. It can be estimated as $W \sim I_c^2 R_{\rm N} \approx 10\,{\rm nW}$ per junction, where we have taken typical values $I_c = 0.1$ mA for the critical current of the junction and $R_{\rm N} = 1\Omega$ for its shunt resistance. Thus the dissipated power can be traded for speed by decreasing I_c. This is because the switching time t_{del} of the Josephson junction is a inverse function of I_c: $t_{\rm del} = \Phi_0/(I_c R_{\rm N}) \approx 20\,{\rm ps}$. To make RSFQ junction resistors remaining normal (non-superconducting) at millikelvin temperatures it is feasible to use the Au-Pd resistor process recently developed at the Hypres foundry instead of conventional Mo resistors.

Unfortunately the critical current can not be decreased too much. At temperature $T = 4.2\,{\rm K}$ the error rate of RSFQ logic $\gamma \approx \gamma_{\rm th} = 2\pi k_{\rm B} T/(I_c \Phi_0)$ is limited by thermal fluctuations. The quantum effects in RSFQ junctions also lead to errors [23,24] which are characterized by the rate $\gamma_{\rm qu} = 2\pi e R_{\rm N}/\Phi_0$. At $T = 4.2$ K the rate $\gamma_{\rm qu}$ is of the same order of magnitude as $\gamma_{\rm th}$. Thus at millikelvin temperatures the minimum critical current of the junctions will be determined by the quantum fluctuations.

Bias resistors are usually placed on the same chip. Moving them from the millikelvin to, say, 1 K stage of a dilution refrigerator allows us to significantly decrease the power dissipation of RSFQ circuits at low temperatures. The power budget of the RSFQ circuit tested here was determined by 17 bias resistors placed on the same chip as the vortex qubit. The total dissipated power in these resistors was about $\sim 7.5\,\mu$W. For future measurements in the quantum regime at $T < 50$ mK *all* bias resistors can be moved to 1 K stage and their wiring to the quantum chip can be made using superconducting wires which do not dissipate any power.

It is important to note that, when waiting in a reset state for a vortex to arrive at the SFQ counter, the RS-Flip-Flop circuit does not dissipate any energy. In the idle (reset) state there is no Josephson junction with voltage across it. Thus, for the proposed measurement scheme there will be no dissipating junctions on chip during quantum-coherent evolution of the qubit. The readout of the qubit is performed after the superposition state is stored by rising the barrier, i.e. when the qubit quantum state is projected onto the two localized states. In order not to overheat the qubit by junctions going resistive in the RS-Flip-Flop, the flip-flop has to be quickly reset back to the superconducting (waiting) state and the next qubit operation cycle should start with sufficient delay (some milliseconds) after that.

In summary, the test results described above demonstrate that superconducting RSFQ logic is a very suitable choice for an interface between vortex qubits and room-temperature electronics. RSFQ elements can be used to set the initial state of vortex qubit and read out its final state after the quantum operation. Experiments at millikelvin temperatures should be the next step to verify the made above proposal in quantum regime.

We would like to thank A. Kemp and A. Wallraff for useful discussions.

References

1. Y. Makhlin, G. Schön, A. Shnirman, Rev. Mod Phys. **73**, 357 (2001)
2. D. Vion, A. Aassime, A. Cottet, P. Joyez, H. Pothier, C. Urbina, D. Esteve, M. H. Devoret, Science **296**, 886 (2002)
3. Yang Yu, S. Han, X. Chu, S. Chu, Z. Wang, Science **296**, 889 (2002)
4. J.M. Martinis, S. Nam, J. Aumentado, C. Urbina, Phys. Rev. Lett. **89**, 117901 (2002)
5. Y. Nakamura, Y.A. Pashkin, J.S. Tsai, Nature **198**, 786 (1999)
6. Y. Nakamura, Yu.A. Pashkin, J.S. Tsai, Phys. Rev. Lett. **87**, 246601 (2001)
7. Y. Nakamura, Yu.A. Pashkin, T. Yamamoto, J.S. Tsai, Phys. Rev. Lett. **88**, 047901 (2002)
8. J.R. Friedman, V. Patel, W. Chen, S.K. Tolpygo, J.E. Lukens, Nature **6791**, 44 (2000)
9. C.H. van der Wal, A.C.J. ter Haar, F.K. Wilhelm, R.N. Schouten, C.J. P.M. Harmans, T.P. Orlando, S. Lloyd, J.E. Mooij, Science **290**, 773 (2000)
10. I. Chiorescu, Y. Nakamura, C.J.P.M. Harmans, J.E. Mooij, Science **299**, 186 (2003)
11. A. Wallraff, Y. Koval, M. Levitchev, M.V. Fistul, A.V. Ustinov, J. Low Temp. Phys. **118**, 543 (2000)
12. A. Kemp, A. Wallraff, A.V. Ustinov, Physica C **386**, 324 (2002)
13. A. Kemp, A. Wallraff, A.V. Ustinov, Phys. Stat. Solidi (b) **233**, 472 (2002)
14. T. Kato, M. Imada, J. Phys. Soc. Jpn **65**, 2963 (1996)
15. A. Shnirman, E. Ben-Jacob, B. Malomed, Phys. Rev. B **56**, 14677 (1997)
16. H.S.J. van der Zant, J.F.C. Fritschy, T.P. Orlando, J.E. Mooij, Phys. Rev. Lett. **66**, 2531 (1991)
17. A. Wallraff, A. Lukashenko, J. Lisenfeld, A. Kemp, Y. Koval, M.V. Fistul, A.V. Ustinov, Nature **425**, 155 (2003)
18. K.K. Likharev, V.K. Semenov, IEEE Trans. Appl. Superc. **1**, 3 (1991)
19. A.V. Ustinov, Physica D **123**, 315 (1998)
20. A.V. Ustinov, Appl. Phys. Lett. **80**, 3153 (2002)
21. WinS, Schematic Editor and Circuit Simulator, published at `http://www.kapl.net` (October 2000)
22. Hypres Inc., Elmsford, NY 10523, USA (`http://www.hypres.com`)
23. T. Filippov, JETP Lett. **61**, 858 (1995)
24. T.J. Walls, T.V. Filippov, K.K. Likharev, Phys. Rev. Lett. **89**, 217004 (2002)